

A Heat Kernel based Cortical Thickness Estimation Algorithm

Gang Wang^{1,2}, Xiaofeng Zhang¹, Qingtang Su¹, Jiannong Chen³, Lili Wang¹, Yunyan Ma⁴, Qiming Liu¹, Liang Xu², Jie Shi², and Yalin Wang²

1. School of Computer Science and Technology, Ludong University, P.R.China
2. School of Computing, Informatics, and Decision Systems Engineering, Arizona State University, USA
3. School of Physics & Photoelectric, Ludong University, P.R.China
4. School of Mathematics & Statistics Science, Ludong University, P.R.China

Abstract. Cortical thickness estimation in magnetic resonance imaging (MRI) is an important technique for research on brain development and neurodegenerative diseases. This paper presents a heat kernel based cortical thickness estimation algorithm, which is driven by the graph spectrum and the heat kernel theory, to capture the grey matter geometry information in the *in vivo* brain MR images. First, we use the harmonic energy function to establish the tetrahedral mesh matching with the MR images and generate the Laplace-Beltrami operator matrix which includes the inherent geometric characteristics of the tetrahedral mesh. Second, the isothermal surfaces are computed by the finite element method with the volumetric Laplace-Beltrami operator and the direction of the streamline is obtained by tracing the maximum heat transfer probability based on the heat kernel diffusion. Thereby we can calculate the cerebral cortex thickness information between the point on the outer surface and the corresponding point on the inner surface. The method relies on intrinsic brain geometry structure and the computation is robust and accurate. To validate our algorithm, we apply it to study the thickness differences associated with Alzheimer’s disease (AD) and mild cognitive impairment (MCI) on the Alzheimer’s Disease Neuroimaging Initiative (ADNI) dataset. Our preliminary experimental results in 151 subjects (51 AD, 45 MCI, 55 controls) show that the new algorithm successfully detects statistically significant difference among patients of AD, MCI and healthy control subjects. The results also indicate that the new method may have better performance than the Freesurfer software.

keywords: Cortical thickness, Heat Kernel, Tetrahedral Mesh, Streamline, False Discovery Rate

1 Introduction

Alzheimer’s disease (AD) is a common central nervous system degenerative disease. Its symptoms on clinical anatomy are the partly atrophy in the cerebral cortex of the patients. If we can accurately estimate the cortical thickness and

identify out reliable different regions between patient and control groups, it may help the early detection of the disease, evaluate disease burden, progression and response to interventions. However, despite evidence that medial temporal atrophy is associated with AD progression, the MRI imaging measurement of medial temporal atrophy is still not sufficiently accurate on its own to serve as an absolute diagnostic criterion for the clinical diagnosis of AD at the mild cognitive impairment (MCI) stage.

According to the geometric properties of the measurement tools, the thickness estimation methods can be broadly divided into two categories: based on either surface or voxel characteristics (as reviewed in [1]). The measurement methods based on the surface features are aimed to establish triangular mesh models in accordance with the topological properties of the inner and outer surface, and then use the deformable evolution model to couple the two opposing surfaces. The thickness is defined as the value of the level set propagation distance between the two surfaces. This measurement accuracy can reach the sub-pixel level but requires constantly correcting the weights of various evolutionary parameters to ensure the mesh regularity. Sometimes the model can not work in the high folding regions such as the sulci. Various approaches were proposed to address this problem and increase the thickness estimation accuracy in the high curvature areas. For example, Mak-Fan et al. modeled the sulci regional by adding the cortex thickness constraints [2]. Fischl and Dale proposed to model the middle part of the sulci by imposing the self-intersection constraints [3]. Although better measurement results are achieved, the computation cost is high [4]. The voxel-based method is the measurement on a three-dimension cubic voxel grid. There is no correction of the mesh topology regularity, so the calculation is simple [5, 6]. However, due to the restrictions of the grid resolution, the measurement accuracy is low and sensitive to noise [7]. The voxel-based measurement acquires the cortex thickness information by solving partial differential equations in the potential field, for example, Jones et al. [8] first used the Laplace equation to characterize the layered structure of the volume between the inner and outer surfaces and obtained the stream line. This method is known as the Lagrangian method. Hyde et al. [9] proposed the Euler method by solving the one-order linear partial differential equations for thickness calculation which can improve the computation efficiency. The main disadvantage of the voxel-based estimation method is the computational inaccuracy on the discrete grid. The limited grid resolution affects the accuracy of the thickness measurement. Some prior work, e.g.[10], used the boundary topology to initialize a sub-voxel resolution surface and correct the direction of the stream line. This method can increase the measurement accuracy.

From the above discussion, in order to improve the computational efficiency and the degree of automation, one may expect the choice of voxel-based measurement algorithm is more feasible. However, we should overcome the defect of the limited grid resolution which can not precisely characterize the curved cortical surfaces from MR images. The 3D model we need should achieve a good fitting for the cerebral cortex morphology and facilitate an effective computation on the sub-voxel resolution. The preferred model to satisfy the above requirements

is a tetrahedral mesh [11], as a cubic voxel can be divided into n tetrahedra according to the resolution requirement.

It is also worth noticing that the tetrahedral mesh quality will affect the accuracy of solving the partial differential equations. For example, too small dihedral angles will lead to stiffness matrix ill-posed problem in the finite element method and too large dihedral angles will lead to the interpolation and discretization errors. The common tetrahedra generation method is to revise the tetrahedra through the iterative processing. One class of methods are to divide the voxels of the MRI to tetrahedra according to the generation quality [12]. But it usually results in the loss of the original image information because of the lack of the boundary restriction conditions. Another class of methods intends to comply with the precise topology structure of the original image by adaptively adjusting the size of the tetrahedra [13], which constantly use the external force to pull the tetrahedral vertices to the boundary of the MRI. However, it neglects the quality of each tetrahedron.

There are two main contributions in our paper. First, this paper intends to generate the high-quality tetrahedral mesh suitable for the areas of the cortex with rich details on the basis of the results of the previous studies. And the tetrahedral mesh can be facilitated to analyze the potential field, which has been elaborated in many literatures, e.g. [14]. Compared with prior work [8], our PDE solving computation can achieve sub-voxel accuracy. Second, we propose a heat kernel based method to accurately estimate the streamline with the intrinsic and global cortical geometry information. In a prior work [8], the computations of the streamline by solving the partial differential equations are rooted in computational geometry to determine the streamline directions. It neglects the inherent geometric characteristics between the points in the mesh. Geometrically speaking, heat kernel determines the intrinsic Riemannian metric [15] and it can be reliably computed through the Laplace-Beltrami matrix. Recently, the surface based heat kernel methods were widely used in image shape analysis [16], classification [17], and registration [18]. However, 3D heat kernel methods are still rare in medical image analysis field. Here we propose a novel 3D heat kernel method and apply it to refine streamline computation and improve the accuracy of the cortical thickness estimation. Besides the computational efficacy and efficiency, our method also takes numerous other advantages of the spectral analysis such as the measurement invariance of inelastic deformation and the robustness of the topological noise.

2 Tetrahedral mesh generation algorithm

The pipeline of our tetrahedral mesh generation algorithm for the MR images is shown in Fig. 1. First we fill the MRI space with the cubic background voxels and the space attribute of each vertex is determined by the point-to-boundary distance function $\phi(x)$. $\phi(x)$ is calculated using the fast marching method based on the vertex connection relationship. The sign of the $\phi(x)$ indicates the region where the vertex is located, and mark the square surface as the boundary where the $\phi(x)$ of vertices is equal to zero. Here we can adaptively adjust the filled cubic

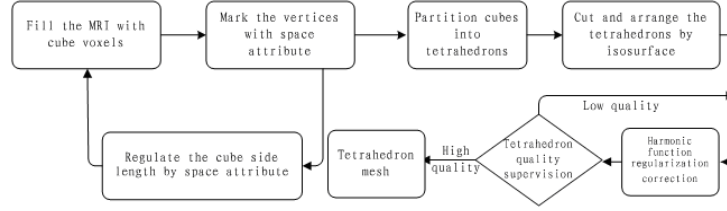
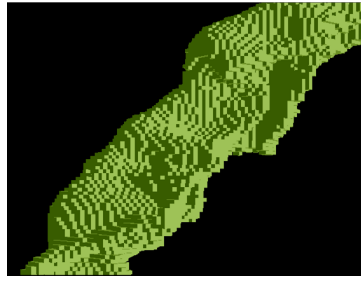


Fig. 1: Tetrahedral mesh generation work flow.



(a) cubic side length as 0.23mm



(b) cubic side length as 0.04mm

Fig. 2: Generated tetrahedral meshes with different cubic side lengths.

lengths by calculating the vertex coordinates(x or y) difference of the adjacent boundary surface with the same z coordinate.

The results of different cubic length are shown in Fig. 2. We adaptively adjust the cubic side lengths to fill the MRI according to the vertices fluctuation of the cubes. On the other hand, the degree of the approximation and smoothness of the mesh can be adaptively adjusted. Secondly, the cubic voxel containing the boundary surface and the internal voxel are split into the tetrahedra according to the pyramid and the body-centered lattice forms. The details of the splitting algorithm are shown in Fig. 3. Here, the left voxel contains the boundary surface (ABCD), O and O' are the central points of the left and right cubic voxels, the tetrahedra (ABDO and BDCO) are the split results by the pyramid form. And the right voxel is the internal one, the tetrahedra (OO'EF and OO'GH) are the split results by the body-centered lattice form. So the cubic voxels are composed of excellent quality tetrahedra, which have dihedral angles as 60° and 90° .

On this basis, the tetrahedra near the boundary are to be cut by the isosurface ($\phi(x) = 0$) based on the vertex space attribute and linear proportional function. Finishing the cutting, we should consider the reconstruction of the new tetrahedra under the condition of the original tetrahedral collapse. In addition,

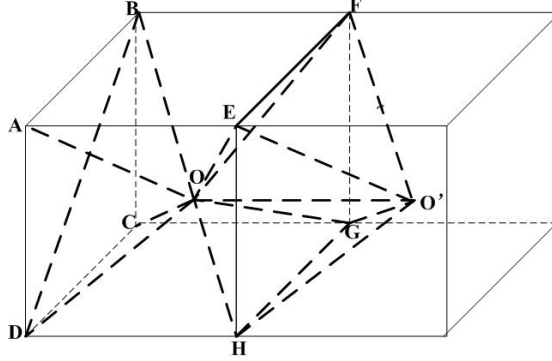


Fig. 3: Two kinds of forms for splitting the cubic voxels into tetrahedra.

if we find the cutting point of the edge is close to the holding internal vertex, the implementation of adsorption operation is required, i.e. the internal vertex will be pulled onto the isosurface. After the above operations, the original background grid is organized into the tetrahedral mesh which substantially fits the cerebral cortex geometry structure.

The obtained tetrahedral mesh needs to be corrected to improve the quality and the smoothness owing to the cutting and organization operations. We achieve it with the regularization algorithm for the boundary smoothness and tetrahedral quality improvement based on the harmonic function minimization [19]. The initial tetrahedra conforming state is given by X , while the deformed state is denoted by x , and the displacement vector field v is given by $v = x - X$. Then the regularized tetrahedral mesh is obtained by finding a v that minimizes an energy $G(v)$. $G(v)$ is composed of three additive terms, an elastic term $E(v)$, a smoothness term $S(v)$ and a fidelity term $B(v)$. The details of this algorithm can be referred to [19].

3 Thickness measurement algorithm based on the heat kernel diffusion

3.1 Heat Kernel

Let f be a real-valued function, with $f \in \mathbb{C}^2$, defined on a tetrahedral mesh K . We use the volumetric Laplace-Beltrami operator proposed in a prior work [20]. We define the piecewise Laplace-Beltrami operator as the linear operator $\Delta_K : C^{PL} \rightarrow C^{PL}$ on the space of piecewise linear function f , on K , which is defined as

$$\Delta_K(f) = \sum_{\{u,v\} \in K} k(u,v)(f(u) - f(v)) \quad (1)$$

where $k(u,v) = \frac{1}{12} \sum_{i=1}^n l_i \cot(\theta_i)$, θ_i is the associated dihedral angle and l_i is the length of an edge to which edge $\{u,v\}$ is against in a tetrahedron model.

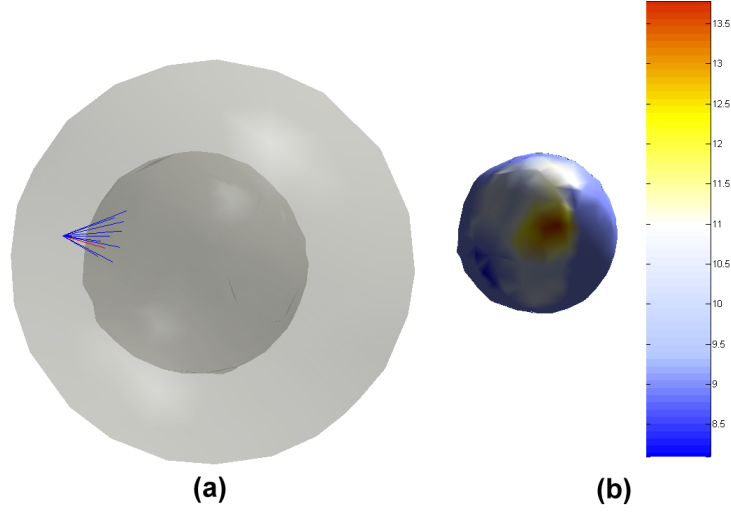


Fig. 4: The heat transition paths and the values of the from the specific point on the outer isothermal surface (0.95°) to the different points on the inner isothermal surface (0.90°).

Compared with other rasterization-based Laplace-Beltrami operator computation methods, because of the multi-resolution nature of the tetrahedral mesh, our method may capture and quantify local volumetric geometric structure more accurately.

The heat kernel diffusion on differentiable manifold with Riemannian metric is governed by the heat equation:

$$\Delta_K f(x, t) = \frac{\partial f(x, t)}{\partial t} \quad (2)$$

where $f(x, t)$ is the heat distribution of the volume at the given time t . We know that the heat diffusion process can be represented by its time dependent and its spatially dependent parts.

$$f(x, t) = F(x)T(t) \quad (3)$$

When Eq. 3 is substituted to Eq. 2, we can get the Helmholtz equation to describe the heat vibration modes in the spatial domain.

$$\Delta F(x) = -\lambda F(x) \quad (4)$$

Eq. 4 can be treated as the Laplacian eigenvalue problem with infinite number of eigenvalue λ_i and eigenfunction F_i pairs. The solution of equation above can be interpreted to the superposition of the harmonic functions in the given spatial position and time. Given an initial heat distribution $F : K \rightarrow \mathbb{R}$, let $H_t(F)$ denote the heat distribution at time t , and $\lim_{t \rightarrow 0} H_t(F) = F$. H_t is called the heat operator. Both Δ_K and H_t share the same eigenfunctions, and if λ_i is an

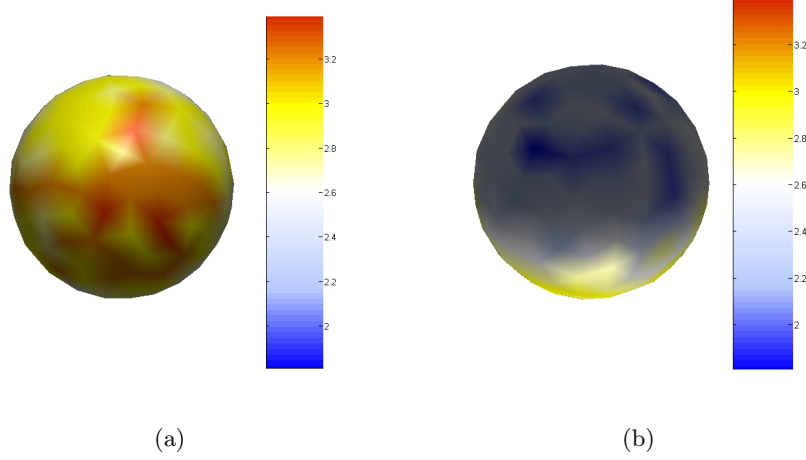


Fig. 5: The thickness measurement result from Fig. 4. (a) shows that the half outer surface which is far from the inner hole and (b) shows the half outer surface which is close to the inner hole. The colormap information represents the size of the thickness.

eigenvalue of Δ_K , then $e^{-\lambda_i t}$ is an eigenvalue of H_t corresponding to the same eigenfunction.

For any compact Riemannian manifold, there exists a function $k_t(x, y) : \mathbb{R}^+ \times M \times M \rightarrow \mathbb{R}$, satisfy the formula

$$H_t F(x) = \int_K k_t(x, y) F(y) dy \quad (5)$$

where dy is the volume form at $y \in K$. The minimum function $k_t(x, y)$ that satisfies Eq. 5 is called the *heat kernel*, and can be considered as the amount of heat that is transferred from x to y in time t given a unit heat source at x . According to the theory of the spectral analysis, the heat kernel has the following eigen-decomposition heat diffusion distance:

$$k_t(x, y) = \sum_{i=0}^{\infty} e^{-\lambda_i t} \phi_i(x) \phi_i(y) \quad (6)$$

where λ_i and ϕ_i are i th the eigenvalue and eigenfunction of the Laplace-Beltrami operator, respectively. So we can see that the heat kernel can be completely represented by the eigenvalues and eigenfunctions of the Laplace-Beltrami operator. At the same time, the heat kernel $k_t(x, y)$ can be interpreted as the transition probability of the Brownian motion on the manifold and has significant applications in computer vision and machine learning fields. The $k_t(x, y)$ of the specific point x on an isothermal surface m to the different point y on the next isothermal surface m' at the same time interval can represent the different heat transition probability. The connection direction of the x and y according to the maximum transition probability is the direction of the temperature gradient. And then y as a starting point, we will continue to search the next point y' in the next

isothermal surface n whose $k_t(x, y)$ is the maximum among the all $k_t(y, \mathbb{R})$. So a streamline of the cortex will be obtained by finding out the maximum heat transition probability between the isothermal surfaces in the order from the specific point on the highest isothermal surface.

3.2 Heat Transition Path

In this paper, we use the Laplace equation in the cortex region to obtain the temperature distribution by the finite element method. The $k_t(x, y)$ of the specific point x on an isothermal surface m to the different point y on the next isothermal surface m' at the same time interval is computed. In the following, we make a simulation experiment to measure the thickness. A hollow shell is generated by our tetrahedron mesh generation algorithm. The outer surface center is located in $(-0, 0, 0)$ and the inner surface center is $(-0.5, 0, 0)$, the outer surface and the hole surface are the irregular spherical surfaces. First we set the temperature value of the outer surface as 1° and inner surface as 0° . Through the finite element method, the temperature distribution and the isothermal surface in the mesh can be acquired. Fig. 4(a) shows that the coordinates of x are $(-3.9669, 0.49833, 0.12544)$ on the outer isothermal surface m whose temperature is 0.95° , and the inner isothermal surface m' is the surface of temperature of 0.90° . The part of heat transition paths from x to the isothermal surface m' are represented by the blue lines. Where the red line represents the path from x to y whose coordinates are $(-1.9645, 0.26586, 1.0978)$ and the maximum $k_t(x, y)$ is 13.081 as the time interval is 0.02. And the important point is that the red line is perpendicular to the two isothermal surfaces approximately. In order to clearly show the heat transition paths, the interval distance between the two isothermal surfaces is enlarged to display. Fig. 4 (b) shows the values of the $k_t(x, y)$ on the inner isothermal surface from x to the different y . As shown in Fig. 4 (a) and (b), we can see that the values of $k_t(x, \mathbb{R})$ increase as the colors go from blue to yellow and to red. This means the geometry and topology relationships from x to the different points on the next isothermal surface. With this simple example, we visualize the fact that eigenvalues and eigenfunctions of the Laplace-Beltrami Operator can represent the intrinsic volume geometry characteristics.

Some thickness measurement results from Fig. 4 are shown in Fig. 5. Here the step size is chosen as 0.2 which means that the isothermal interval is 0.2° . We add the length of all the segment lines between the isothermal surfaces which represent the maximum heat transition and obtain the thicknesses of the vertices on the outer surface. Fig. 5 (a) shows that the half outer surface which is far from the hole and (b) shows the half outer surface which is close to the hole. The colormap information represents the size of the thickness.

4 Statistical Maps and Multiple Comparison

The experiments in this work were performed on T1 image data (AD=51, MCI=45, control=55) from the Alzheimer's Disease Neuroimaging Initiative (ADNI) [21]. As a proof-of-principle work, our analysis was focused on the medial temporal

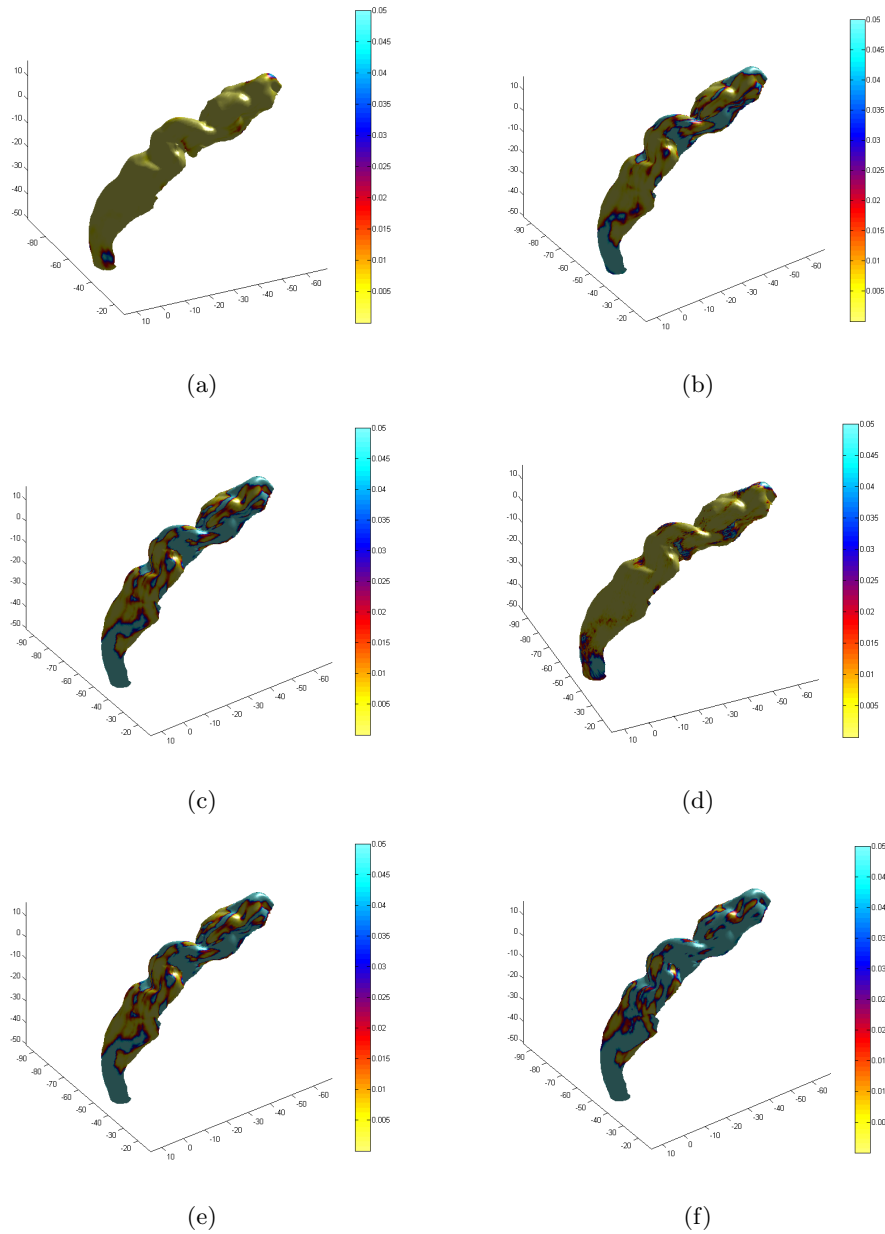


Fig. 6: Statistical p-map results of Heat Diffusion and Freesurfer show group differences among three different groups, (a), (c), (e) are the results of our method, (b), (d), (f) are results of Freesurfer software on group difference between AD and control, control and MCI, AD and MCI, respectively.

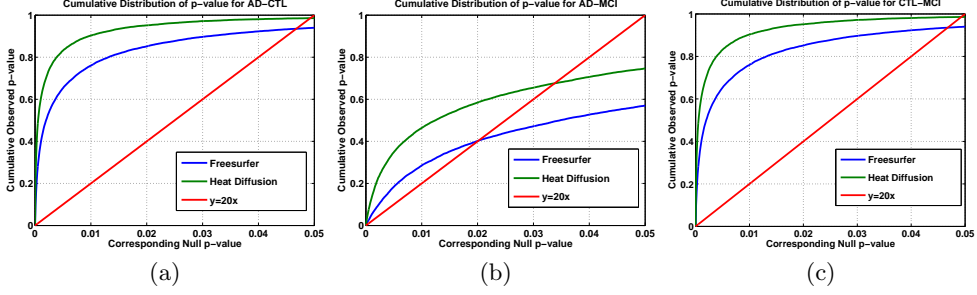


Fig. 7: The cumulative distributions of p-values comparison for difference detected between three groups (AD, MCI, CTL). In the CDF, the q-values are the intersection point of the curve and the $y = 20x$ line. In a total of 3 comparisons, the heat diffusion method achieved the highest q-values.

lobe of the left brain hemisphere. The grey matter segmentation, surface reconstruction, surface correspondence, region of interest (ROI) extraction on white matter and pial surfaces were computed by Freesurfer software [22].

With the segmented brain images, the acquired data was interpolated to form cubic voxels with an edge length of 0.2mm. The minimum dihedral angle of the generated tetrahedron mesh is 12 degree and maximum dihedral angle is 130 degree. The maximum edge ratio is set as 5.0. Then the thickness measurement based on heat kernel is applied on the extracted ROI. We applied the Student's t test on sets of thickness values measured on corresponding surface points to study the statistical group difference. Given each matching surface point, we measure the difference between the mean thickness of three different groups (AD vs. control, MCI vs. control and AD vs. MCI) by

$$t = \frac{\bar{U} - \bar{V}}{\sqrt{\frac{2}{n} S_{UV}}} \quad (7)$$

where \bar{U} and \bar{V} are the thickness means of the two groups and S_{UV} is the grand standard deviation. The denominator of t is the standard error of the difference between two means. For multiple comparison, we ran a permutation test with 15,000 random assignments of subjects to groups to estimate the statistical significance of the thickness with group differences. The covariate was permuted 15,000 times. The probability was later color coded on each surface template point as the statistical p -map of group difference. Fig. 6 shows the p -maps of group difference detected between AD and control, AD and MCI, control and MCI groups, respectively, and the significant level at each surface template point as 0.05. Fig. 6 (a), (c) and (e) are the statistical p -map results with Heat Diffusion; (b), (d) and (f) are those with Freesurfer. All group difference p -maps were corrected for multiple comparisons using the widely-used false discovery rate method (FDR) [23]. The FDR method decides whether a threshold can be assigned to the statistical map that keeps the expected false discovery rate below 5% (i.e., no more than 5% of the voxels are false positive findings). In Fig. 6, the

	Heat kernel diffusion	Freesurfer
AD-CTL	0.0492	0.0459
AD-MCI	0.0347	0.0201
CTL-MCI	0.0425	0.0348

Table 1: The FDR corrected p -value (q -value) comparison.

non-blue color areas denote the statistically significant difference areas between two groups. Fig. 7 (a)-(c) are the cumulative distribution function (CDF) plots showing the uncorrected p -values (as in a conventional FDR analysis). The x value at which the CDF plot intersects the $y = 20x$ line represents the FDR-corrected p -value or q -value. It is the highest statistical threshold that can be applied to the data, for which at most 5% false positives are expected in the map. In general, a larger q -value indicates a more significant difference in the sense that there is a broader range of statistic threshold that can be used to limit the rate of false positives to at most 5% [24]. The use of the $y = 20x$ line is related to the fact that significance is declared when the volume of suprathreshold statistics is more than 20 times that expected under the null hypothesis.

With the proposed univariate statistics, we studied differences between three diagnostic groups: AD, MCI and controls. As expected, we found relatively strong thickness differences between AD and control groups (q -value: 0.0492 with heat diffusion method and 0.0459 with Freesurfer software) and strong thickness differences between MCI and control groups (q -value: 0.0425 with heat diffusion method and 0.0348 with Freesurfer software), the details are in Fig. 6 and Fig. 7. We compared the statistical power (determined by FDR corrected overall significant values) with the two thickness methods, our method demonstrated the strongest or comparable statistical power for the three group comparisons (detailed in Table 1). Although more validation is certainly necessary, the current results suggest that the heat diffusion measure may offer greater statistical power than the Freesurfer software.

5 Conclusion

In this paper, we present a heat kernel based thickness estimation algorithm which can improve the computational efficiency and accuracy for *in vivo* MR image cortical thickness estimation. Through establishing the tetrahedral mesh matching with the MRI by the harmonic energy function, we can reduce the limited grid resolution effects. At the same time, we introduce the heat kernel to the streamline analysis to determine the heat transfer gradient direction. With the proposed univariate statistics, we studied differences between three diagnostic groups: AD, MCI and controls. We compare our method with the Freesurfer software, the results show that the heat diffusion method achieved greater statistical power than the Freesurfer software in a total of three comparisons. In the future, we plan to depict the geometrical characteristics of the local and global cortical regions by using the heat kernel diffusion and apply them in our ongoing preclinical AD research.

6 Acknowledgments

This work was supported by the National Natural Science Foundation of China (No. 11074105), , the Science and Technology Development Program of Shandong Province (No. 2011YD01078), the Natural Science Foundation of Shandong Province (No. ZR2012FL21). the School-Enterprise Fund of Ludong University (No. 2010HX007).

References

1. Clarkson, M.J., Cardoso, M.J., Ridgway, G.R., Modat, M., Leung, K.K., Rohrer, J.D., Fox, N.C., Ourselin, S.: A comparison of voxel and surface based cortical thickness estimation methods. *Neuroimage* **57**(3) (Aug 2011) 856–865
2. Mak-Fan, K.M., Taylor, M.J., Roberts, W., Lerch, J.P.: Measures of cortical grey matter structure and development in children with autism spectrum disorder. *J Autism Dev Disord* **42**(3) (Mar 2012) 419–427
3. Fischl, B., Dale, A.M.: Measuring the thickness of the human cerebral cortex from magnetic resonance images. *Proc. Natl. Acad. Sci. U.S.A.* **97**(20) (Sep 2000) 11050–11055
4. Dahnke, R., Yotter, R.A., Gaser, C.: Cortical thickness and central surface estimation. *Neuroimage* **65** (Jan 2013) 336–348
5. Cardoso, M.J., Clarkson, M.J., Ridgway, G.R., Modat, M., Fox, N.C., Ourselin, S.: LoAd: a locally adaptive cortical segmentation algorithm. *Neuroimage* **56**(3) (Jun 2011) 1386–1397
6. Scott, M.L., Bromiley, P.A., Thacker, N.A., Hutchinson, C.E., Jackson, A.: A fast, model-independent method for cerebral cortical thickness estimation using MRI. *Med Image Anal* **13**(2) (Apr 2009) 269–285
7. Das, S.R., Avants, B.B., Grossman, M., Gee, J.C.: Registration based cortical thickness measurement. *Neuroimage* **45**(3) (Apr 2009) 867–879
8. Jones, S.E., Buchbinder, B.R., Aharon, I.: Three-dimensional mapping of cortical thickness using Laplace’s equation. *Hum Brain Mapp* **11**(1) (Sep 2000) 12–32
9. Hyde, D.E., Duffy, F.H., Warfield, S.K.: Anisotropic partial volume CSF modeling for EEG source localization. *Neuroimage* **62**(3) (Sep 2012) 2161–2170
10. Jones, G., Chapman, S.: Modeling growth in biological materials. *SIAM Review* **54**(1) (2012) 52–118
11. Cassidy, J., Lilge, L., Betz, V.: Fullmonte: a framework for high-performance monte carlo simulation of light through turbid media with complex geometry. (2013) 85920H–85920H–14
12. Liu, Y., Xing, H.: A boundary focused quadrilateral mesh generation algorithm for multi-material structures. *Journal of Computational Physics* **232**(1) (2013) 516–528
13. Lederman, C., Joshi, A., Dinov, I.: Tetrahedral mesh generation for medical images with multiple regions using active surfaces. In: *Proc IEEE Int Symp Biomed Imaging*. (2010) 436–439
14. Liu, Y., Foteinos, P.A., Chernikov, A.N., Chrisochoides, N.: Mesh deformation-based multi-tissue mesh generation for brain images. *Eng. Comput. (Lond.)* **28**(4) (2012) 305–318
15. Zeng, W., Guo, R., Luo, F., Gu, X.: Discrete heat kernel determines discrete riemannian metric. *Graph. Models* **74**(4) (July 2012) 121–129

16. Chung, M.K., Robbins, S.M., Dalton, K.M., Davidson, R.J., Alexander, A.L., Evans, A.C.: Cortical thickness analysis in autism with heat kernel smoothing. *NeuroImage* **25**(4) (2005) 1256 – 1265
17. Bronstein, M.M., Bronstein, A.M.: Shape recognition with spectral distances. *IEEE Trans Pattern Anal Mach Intell* **33**(5) (May 2011) 1065–1071
18. Sharma, A., Horaud, R.P., Mateus, D.: 3D shape registration using spectral graph embedding and probabilistic matching. *Image Processing and Analysing With Graphs: Theory and Practice* (2012) 441–474
19. Lederman, C., Joshi, A., Dinov, I., Vese, L., Toga, A., Van Horn, J.D.: The generation of tetrahedral mesh models for neuroanatomical MRI. *Neuroimage* **55**(1) (Mar 2011) 153–164
20. Wang, Y., Gu, X., Chan, T.F., Thompson, P.M., Yau, S.T.: Volumetric harmonic brain mapping. In: *Biomedical Imaging: From Nano to Macro, 2004. ISBI 2004. IEEE International Symposium on.* (Apr. 2004) 1275–1278
21. Mueller, S.G., Weiner, M.W., Thal, L.J., Petersen, R.C., Jack, C., Jagust, W., Trojanowski, J.Q., Toga, A.W., Beckett, L.: The Alzheimer’s disease neuroimaging initiative. *Neuroimaging Clin. N. Am.* **15**(4) (Nov 2005) 869–877
22. Fischl, B., Sereno, M.I., Dale, A.M.: Cortical surface-based analysis II: Inflation, flattening, and a surface-based coordinate system. *NeuroImage* **9**(2) (1999) 195 – 207
23. Nichols, T., Hayasaka, S.: Controlling the familywise error rate in functional neuroimaging: a comparative review. *Stat Methods Med Res* **12**(5) (Oct 2003) 419–446
24. Wang, Y., Shi, J., Yin, X., Gu, X., Chan, T.F., Yau, S.T., Toga, A.W., Thompson, P.M.: Brain surface conformal parameterization with the Ricci flow. *IEEE Trans Med Imaging* **31**(2) (Feb 2012) 251–264